Sound Pressure Level Gain in an Acoustic Metamaterial Cavity

Kyungjun Song[1], Kiwon Kim[2], Shin Hur[1], Jun-Hyuk Kwak[1], Jihyun Park[3], Jong Rak Yoon[3] & Jedo Kim[4]

[1]Department of Nature-Inspired Nanoconvergence Systems, Korea Institute of Machinery and Materials, 156 Gajeongbuk-Ro, Daejeon, 305-343, Korea, [2]Department of Mechanical Engineering, Korea Advanced Institute of Science and Technology, 291 Daehak-Ro, Yuseong-Gu, Daejeon, 305-701, Korea, [3]Signal Processing Laboratory, Department of Information and Communication Engineering, Pukyong National University, 45 Yongso-ro, Nam-Gu, Busan, 608-737, Korea, [4]Department of Mechanical Engineering, Pukyong National University, 365 Sinsun-Ro, Nam-Gu, Busan, 608-739, Korea.

The inherent attenuation of a homogeneous viscous medium limits radiation propagation, thereby restricting the use of many high-frequency acoustic devices to only short-range applications. Here, we design and experimentally demonstrate an acoustic metamaterial localization cavity which is used for sound pressure level (SPL) gain using double coiled up space like structures thereby increasing the range of detection. This unique behavior occurs within a subwavelength cavity that is 1/10th of the wavelength of the incident acoustic wave, which provides up to a 13 dB SPL gain. We show that the amplification results from the Fabry-Perot resonance of the cavity, which has a simultaneously high effective refractive index and effective impedance. We also experimentally verify the SPL amplification in an underwater environment at higher frequencies using a sample with an identical unit cell size. The versatile scalability of the design shows promising applications in many areas, especially in acoustic imaging and underwater communication.

The acoustic attenuation coefficients of common homogeneous viscous media, such as air, water, and metals, show a frequency-squared dependence ($\alpha \propto f^2$); thus, the higher the frequency, the higher the losses[1–3]. In ultrasound imaging, because of the short penetration depth associated with high frequency signals ($>$10 MHz), low frequency signals ($<$10 MHz) is used to scan deep structures[2] and in underwater communications, low frequency signals ($<$1 kHz) is generally used for underwater communication over hundreds of km[3,4]. Nonlinear amplification devices can be used to electronically amplify acoustic signals to compensate for the losses; however, distinguishing the acoustic signal from the background noise becomes very challenging when the sound pressure level (SPL) is near or below the threshold of piezoelectric transducers[1]. One approach to overcoming this problem is to exploit the unique properties of acoustic metamaterials by introducing "obstacles" to constrict or confine sound waves into a small volume[5–10], thereby achieving a "SPL gain". To confine the acoustic energy into a small volume, it is necessary to create a subwavelength region surrounded by a high impedance, Z, and a high index of refraction, n, that provide highly efficient sound entrapment and miniaturization of the device, respectively. However, materials that exhibit both high Z and n values are virtually nonexistent in nature because the speed of sound (c) in a material generally increases with the density (ρ). Acoustic metamaterials are promising candidates for circumventing this fundamental limitation because artificial periodic structures can be manipulated to achieve unprecedented control over sound wave propagation[11–29]. For example, extreme acoustic properties, such as zero density[25], negative density[16,27], negative bulk modulus[18], and negative refractive index[15,19,21,22,24], have been realized by designing artificial periodic structures on the subwavelength scale.

In this study, in contrast to previously realized enhanced sound emissions by our group[30], we extended it to demonstrate SPL gain of an external acoustic signal inside an ultra-small cavity. We achieved this unique behavior by using two parallel slabs composed of periodic corrugated structures. This structure provides an effective sound path, resulting in a high effective refractive index (n_{eff}) and effective impedance (Z_{eff}). As shown below, these effective properties depend on the length of the artificial sound channels in the direction of propagation; thus, the sound localization and resonant frequencies can be controlled by careful design of the structure. The experimental results for three different path lengths are in excellent agreement with the theoretical results, showing up to a 13 dB gain in air. In addition, sound localization in water is demonstrated. Our results indicate that low pressure acoustic signals below the threshold of transducers can be enhanced or amplified to increase the range of detection by being confined in a subwavelength cavity. The designed structure is scalable for any dimension; thus, such acoustic localization cavity can be used to amplify lossy acoustic signals in variety of fields including ultrasonic imaging and underwater communication.

Results

Amplification measurements and sound localization. The acoustic metamaterial cavity that is designed and constructed for this study is shown in Fig. 1a. This sample has dimensions of $10 \times 4.2 \times 13$ cm with a unit cell size, a, of 1 cm. We design three different samples, as shown in Fig. 1b, with identical unit cell sizes but different structures. Thus, different path lengths, l, are obtained by changing the flange length, w. The localization cavity is created using two acoustic metamaterial slabs that are separated by a subwavelength air gap, g, to form a cavity. The stiff corrugated structures form an artificial "zigzag" path along the direction of wave propagation, effectively creating a "coiling-up" space[15,30,31]. Such a structure is ideal for the versatile control of n_{eff} and Z_{eff} because progressively longer paths can be easily realized by elongating the flange length, as can be seen for samples 1 to 3. The amplification rate of the metamaterial cavity is measured in an anechoic chamber (see Fig. S1 in the supplementary materials) using a B&K microphone that is placed inside the cavity to measure the sound pressure level (SPL). We use COMSOL, a finite element software package, to theoretically predict and compare the SPL using the following physical parameters for the structure, density $= 2.7 \times 10^3$ kg/m³, Poisson's ratio $= 0.35$, and Young's modulus $= 70 \times 10^9$ Pa, to simulate aluminum, and air is used as the working fluid. The results in Fig. 1c show that sample 1, which has the highest refractive index, produces the highest gain of up to 13 dB at a fundamental frequency of 990 Hz. This result is in almost agreement with the theoretical prediction. At this frequency, the wavelength is approximately 35 times the periodicity and 10 times the total length of the structure in the direction of wave propagation. The figure shows that progressively lower gains and higher fundamental frequencies are observed for samples 2 and 3 as the path length is reduced by decreasing w. However, the slight decrease in SPL of the experimental result comes from friction loss in the boundary layer[1,31]. If unit cells are reduced to micrometer scale, acoustic resistance can in no way be negligible because device scale is almost comparable to skin depth.

In addition, as the gap size of the cavity is increased, a slight reduction in the SPL is observed. However, the larger volume enabled the longer resonant wavelengths to be confined, thereby shifting the amplification frequency to lower values, as shown in Fig. 1d. The discrepancy of resonant frequencies between experimental and numerical results are attributed to smaller effective cavity volume caused by the insertion of a microphone which is used to detect SPL. The calculated SPL data shown in Figs. 1e and f indicate strong localization within the cavity: the amplification rate increases with the path length but decreases as g is increased. The metamaterial slabs with high Z_{eff} and n_{eff} values on either side of the air gap result in the localization of the fundamental resonance mode within the air gap; however, as the size of the air gap increased, the energy density is reduced. This result shows that higher n_{eff} and Z_{eff} values enhance a sound localization medium by confining the sound into an air gap with a lower n.

Prediction of pressure amplification. We theoretically predict the SPL amplification rate by considering the basic physics of sound transmission through acoustic metamaterials with an air gap and use the effective medium theory, as shown in Fig. 2a. Fig. 2b shows that the SPL amplification is reproduced using a subwavelength cavity that is formed by two effective medium slabs for which the refractive index and the impedance calculated by the numerical scattering method[32,33]. Note that the effective refractive index n_{eff} and Z_{eff} of sample 1 are taken to be $n_{eff} = 4.103$ and $Z_{eff} = 8.445$ (In this work, Z and n are normalized to the background fluid which is air). At the fundamental resonant frequency, sound transmission through the metamaterial cavity is analogous to the well-understood resonant tunneling mechanism for electrons across a double energy barrier or the Fabry-Perot resonance transmission for photons across two opposing flat mirrors. In the long wavelength regime, the proximity of the metamaterial slabs enables the localized sound wave-packet impinging on the wall to couple across the metamaterial, resulting in full transmission through the cavity. At full transmis-
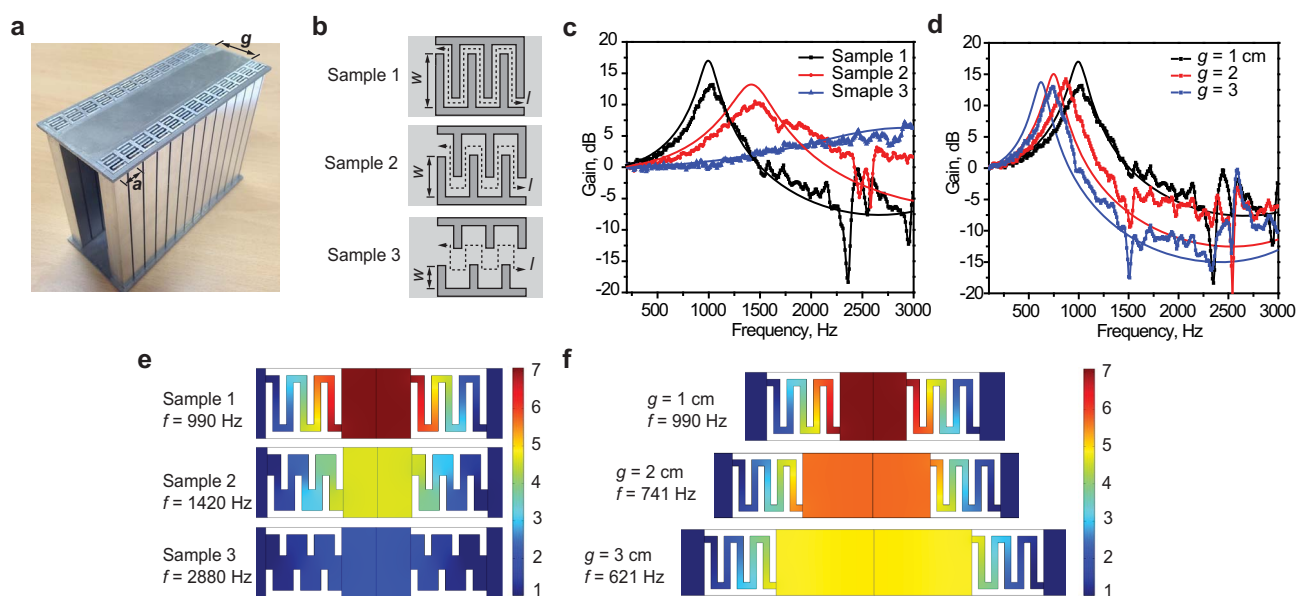
Figure 1 | Amplification rate and sound pressure distribution: (a) acoustic metamaterial cavity composed of double coiled up space like structures with unit cell size, a, of 1 cm used in this study; (b) three samples with progressively shorter path lengths, l, obtained by decreasing the flange length, w (0.7, 0.4, 0.2 cm); (c) experimental (lines with dots) and simulated (lines) sound level gains for samples 1, 2, and 3 with $g = 1$ cm; experimental peak frequency for each sample was $f = 990, 1420,$ and 2880 Hz, respectively; white noise with a frequency range of 71 Hz – 5.65 kHz was used for signal generation; (d) experimental (lines with dots) and simulated (lines) sound level gains for sample 1 with $g = 1, 2,$ and 3 cm; peak frequency for each case was 990, 741, and 621 Hz, respectively; (e) spatial distribution of pressure amplitude for samples 1, 2, and 3 at peak frequencies of 990, 1420, and 2880 Hz, respectively; (f) spatial distribution of pressure amplitude for sample 1 with $g = 1, 2,$ and 3 cm at peak frequencies of 990, 741, and 621 Hz, respectively.
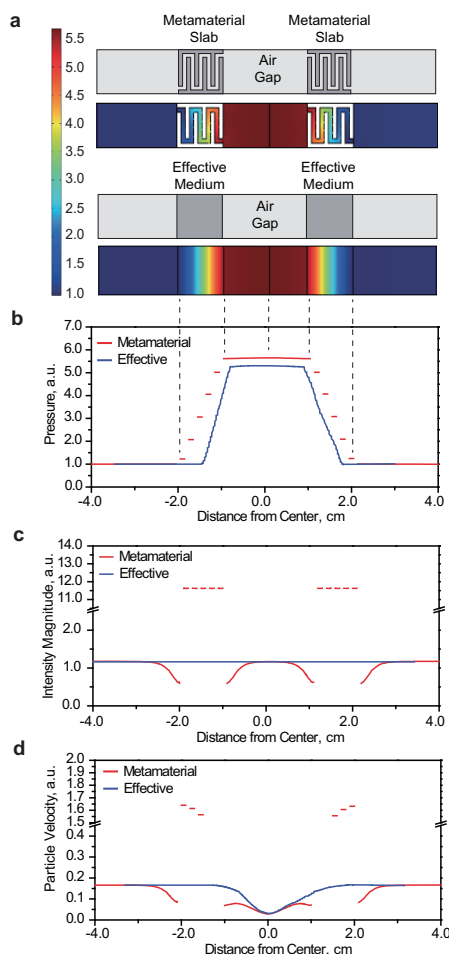
Figure 2 | Theoretical prediction of sound pressure amplification: (a) calculated sound pressure within metamaterial cavity for sample 1 compared with calculated values obtained using effective medium theory; refractive index and impedance of the effective medium were found using a numerical scattering method with transmission data; variations in (b) sound pressure, (c) sound intensity magnitude (RMS), and (d) particle velocity across metamaterial cavity and effective medium cavity.

sion, the sound intensity inside the cavity, I_{cav}, is identical to the incident sound intensity, I_o, as can be seen in Fig. 2c. This result indicates that the energy inside the cavity is not changed by the presence of the acoustic metamaterial cavity. The sound intensity is the product of the sound pressure, P, and the particle velocity, c_p; thus, the sound pressure, P, inside the zigzag metamaterial, P_{cav}, can be expressed as $P_{cav} = I_o/c_p$. This equation shows that for equal sound intensities, the SPL inside the cavity becomes a function of c_p only. Thus, the extraordinary amplification of the SPL originated from the low particle velocity within the cavity and this is shown in Fig. 2d. That is, under these conditions, a standing wave forms inside the metamaterial cavity, and at the fundamental resonance frequency, a displacement node forms at the center, which is the point of maximum pressure variation. Therefore, this configuration can form a first harmonic inside a highly miniaturized cavity, thereby "focusing" the pressure field inside the subwavelength gap. Note that the amplification of the SPL in the gap is controlled by Z_{eff} and n_{eff} because c_p depends on the reflection coefficients of the two walls, which in turn are also determined by Z_{eff} and n_{eff}. Strong Sound confinement inside the air gap can be achieved by high impedance discontinuities between the metamaterial and air. Thus, as the path length is decreased, as is the case for samples 2 and 3, the resulting SPLs are also lowered because of the decrease in Z_{eff} and n_{eff}, as shown in Fig. S2.

Independent control of the refractive index and the impedance. Unlike classical resonators, such as Helmholtz cavities which use acoustic hard walls, the cavity mentioned above is easily miniaturized by increasing the n_{eff} value of the designed metamaterial (because $n_{eff}k_o d = \pi$, where d is the relevant dimension). We expect that a resonator with $Z = 9$ and $n = 4.6$, for example, would provide the same amplification rate as a resonator with $Z = 9$ and $n = 2.3$ but with half the wall thickness. Furthermore, independent control of the impedance and the refractive index are possible by carefully designing the unit cell structure. As an example, we consider three corrugated structures with identical Z_{eff} values (made possible by identical path lengths of 4.6 cm) but different n_{eff} values (see Fig. 3a). As expected, the highest effective refractive index, n_{eff}, and thus the highest effective density, ρ_{eff}, were obtained for case 1 by compressing the zigzag paths into the smallest volume of all of the cases, as shown in Fig. 3b. However, the effective
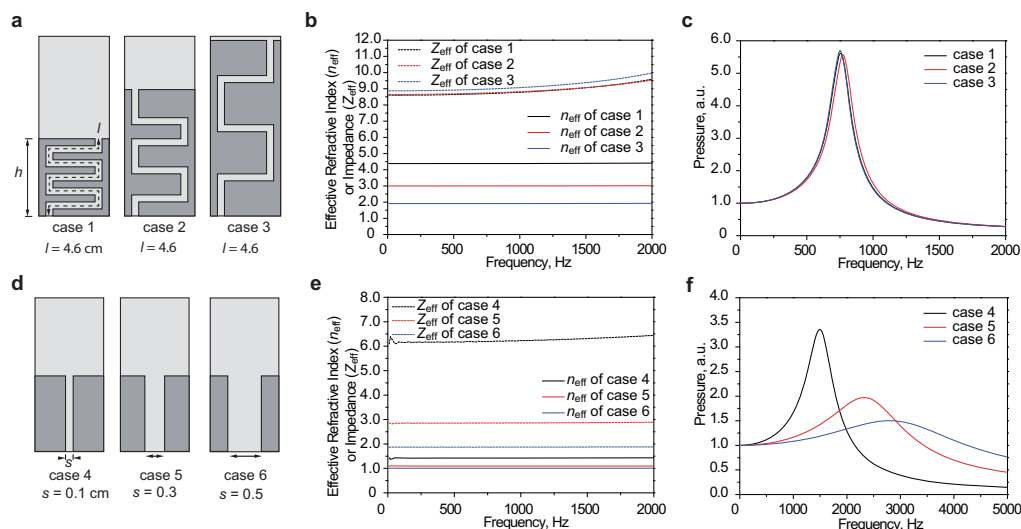

Figure 3 | Independent control of refractive index and impedance: (a) three different corrugated structures used to produce identical path lengths of $l = 4.6$ cm but varying heights, h; (b) effective refractive indices and impedances of the three different structures shown in (a) calculated using acoustic numerical retrieval scattering method; (c) SPL inside the subwavelength cavity for three different metamaterial structures; (d) three different structures with identical heights, h, but varying path widths, w; (e) effective refractive indices and impedances of the three different structures shown in (d); (f) acoustic pressure inside the cavity for three different metamaterial structures.

impedances $Z_{eff} = \rho_{eff}/n_{eff}$ of the three different metamaterial structures are identical, as n_{eff} and ρ_{eff} are increased by the same amount. Thus, Fig. 3c shows that the subwavelength cavities consisting of three different metamaterial designs with identical air gaps of $g = 2$ cm produced the same amplification rates. In contrast, we also considered three different structures with identical n_{eff} values but different Z_{eff} values, which are created by identical thicknesses but different slit width values, s (see Fig. 3d). When the periodicity of the grating is much smaller than the wavelength, λ, only the lowest mode exists inside the metallic slits at constant c_o (where c_o is the speed of sound in the reference material). However, the density $\rho_{eff} = n_{eff}Z_{eff}$ is reduced by the volume fraction of the gaps; thus, the impedance Z_{eff} is reduced as the slit width increased, as shown in Fig. 3e. Case 4 has the largest impedance value among the three cases and thus provided the largest amplification rate at $f = 1500$ Hz, as seen in Fig. 3f. Therefore, we have shown that rather simple alterations in the metamaterial structure can be used to independently control Z_{eff} and n_{eff}, resulting in highly versatile material property control that no conventional materials or systems can mimic.

Enhancing the amplification using quarter-wave resonators. The acoustic meta-material cavity with a double coiled up space like structure that is discussed above is essentially a half-wave resonator in which a standing wave is compressed inside a small effective volume cavity. To further enhance the SPL amplification, we closed off one side of the open cavity with a sound hard wall to form a quarter-wave resonator, as shown in Fig. 4a. Then, the sound hard wall forms a short circuit in the transmission-line model that circulates the acoustic wave to form the following fundamental resonant condition: $L_{cav} = \lambda/4n_{eff}$. Thus, in contrast to the half-wave resonator, a displacement node and a pressure antinode form at the acoustic hard wall. Fig. 4b compares the sound pressure of the half-wave resonator (a cavity with two open ends) and the quarter-wave resonator (a cavity with an open and a closed end), demonstrating enhanced sound amplification at a lower frequency. In Fig. 4c, the intensity of acoustic cavity at resonant frequency is almost zero (simulation results = 0.05) because reflected sound forms a standing wave inside the cavity. However, this extraordinary sound amplification results from the effect of the lower particle velocity, c_p, by the high impedance of an acoustic hard wall, as illustrated in Figs. 4 d, which produces a strong sound pressure amplification $P/P_{in} \simeq 10$ at $g = 1$ cm.

Sound amplification in an underwater environment. We perform additional experiments to show that amplification is also possible underwater using a spherical omnidirectional transducer with a hydrophone placed inside the cavity. The dimensions of the indoor pool are $2 \times 1.5 \times 0.8$ m with no sound-absorbing walls (sound-hard wall), and the distance between the transducer and the cavity is 0.5 m, as shown in Figs. 5 a and b. We closed off one side of the metamaterial cavity to form a quarter-wave resonator to minimize the effect of the interference signals that are created by the non-absorbing walls and the perfectly reflecting surface (water/air interface). We use an LFM (linear frequency modulation) signal with a frequency range from 3 to 25 kHz and a 100-kHz sampling frequency as the source. The results in Fig. 5c show that an acoustic amplification of approximately 3–4 dB is obtained for the sample, which is in excellent agreement with the theoretical predictions. As expected, the gain is relatively low because of the reduction in the impedance mismatch between the metamaterial and the working fluid (water). The signal quality is also relatively poor because of the interference from the tank walls and the water/air interface; however, the acoustic amplification trend is observable. The large size of the hydrophone relative to the wavelength shifts the acoustic gain curve to higher frequencies. That is, the resonance frequency of the sample with a 3-cm gap matches the prediction for the sample with a 2.1-cm gap, which is similar to previous studies with relatively
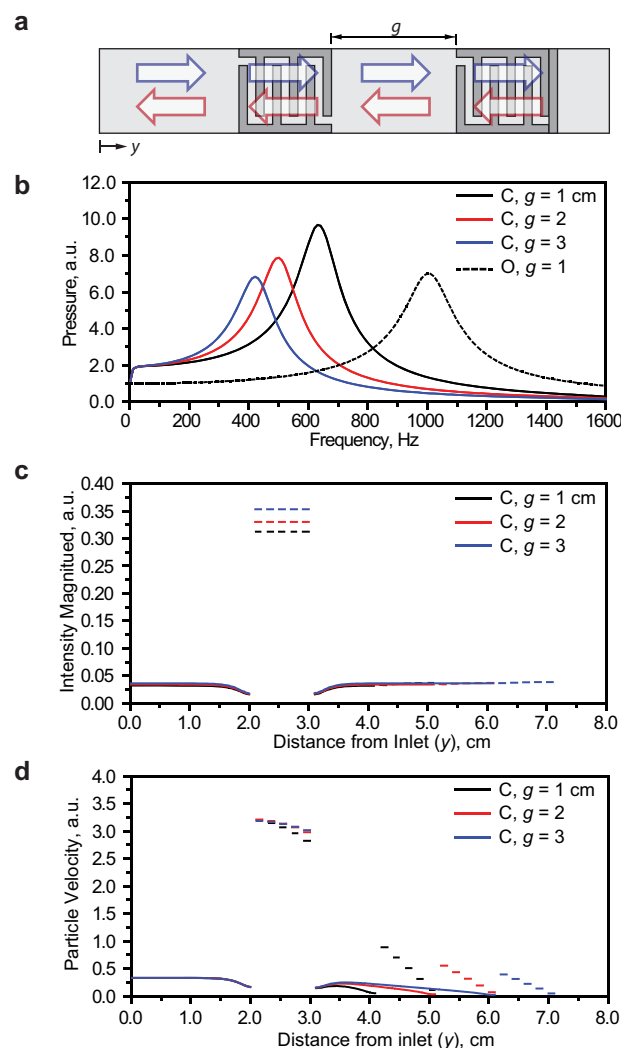

Figure 4 | Enhancing the amplification using a quarter-wave resonator: (a) schematic of metamaterial cavity (Sample 1) with a quarter-wave resonator; incoming acoustic signal was amplified as it was reflected back inside the cavity by an acoustic hard wall; (b) SPLs inside the quarter-wave resonator enhanced the metamaterial cavity with three different gap sizes (C) and the metamaterial cavity with no quarter-wave resonator (O); (c) sound intensity magnitude (RMS), and (d) particle velocity (RMS) across the metamaterial cavity enhanced by the quarter-wave resonator for three different gap sizes.

large inclusions[20]. The calculated SPL exhibits strong sound localization within the cavity at a fundamental frequency of approximately 12 kHz, confirming the potential use of the design for underwater communications and ultrasonic imaging applications.

Discussion
In conclusion, these results show that a subwavelength cavity consisting of acoustic metamaterial slabs with high n_{eff} and Z_{eff} values can be used to achieve an extraordinary SPL gain in a highly localized area. In essence, the prototype amplifies sound pressures up to 13 dB, resulting in an ultra-sensitive acoustic detector that can be used to increase the frequency range of operation of the device. To further increase the amplification rate, various types of unit cells can be designed, and exotic 2D cylindrical and 3D spherical resonators can be used. Additionally, we demonstrate novel independent control of n_{eff} and Z_{eff}, which is unprecedented in conventional materials, thereby paving the way for limitless applications in a variety of
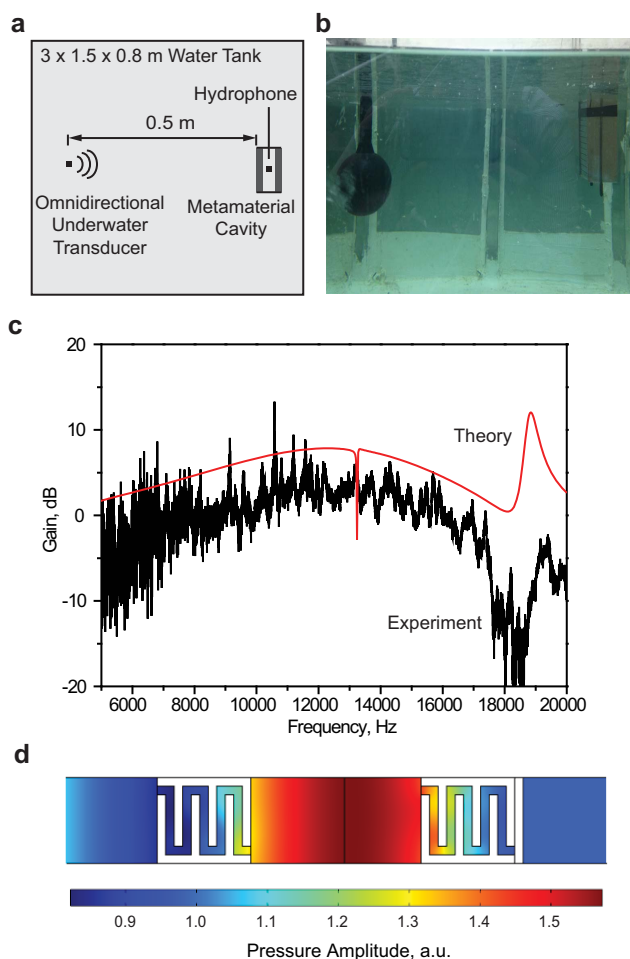
Figure 5 | Sound amplification in an underwater environment:
(a) schematic and (b) photograph of experimental apparatus constructed to measure SPL in an underwater environment; (c) SPL gain for metamaterial sound amplification cavity (Sample 1) enhanced by quarter-wave resonator; (d) calculated SPLs for metamaterial sound amplification cavity enhanced by quarter-wave resonator; COMSOL finite element software was used to simulate SPL using water (ρ = 1000 kg/m³, c = 1480 m/s) as the working fluid.

areas. Furthermore, the versatile scalability of our design enables its usage over wide frequency ranges, which can be applied to ultrasonic transducers and imaging when micro- or nano-fabrication techniques are used.

Methods

Measurement of SPL gain inside the cavity in air. The sound amplification rate inside the cavity was measured by generating an omnidirectional sound pressure by placing a B&K type 4295 speaker in the middle of an anechoic chamber with a cutoff frequency of 100 Hz. The SPL inside the meta-material cavity was measured by a B&K type 4935 microphone, and the reference SPL with no cavity was measured by a B&K type 4189-A-021 microphone (Fig. S1). The two microphones were placed 1.5 m away from the omnidirectional sound speaker. The sound pressure amplification was obtained by calculating the transfer function between the reference SPL and the cavity SPL using a data acquisition device (NI 9234).

Effective acoustic parameters calculation. In order to calculate the refractive index n_{eff} and Z_{eff}, we used the retrieval scattering method based on the reflectance and transmission coefficients obtained by COMSOL Multi-physics software. These coefficients can be calculated by using normally incident sound waves. We invert the scattering coefficients for calculating n_{eff} and Z_{eff} by using constitutive conditions of passive acoustic medium: $\mathrm{Re}(Z) > 0$ and $\mathrm{Im}(n) > 0$.

Amplification Simulations. Numerical simulations were carried out using a COMSOL multi-physics software package. The sound amplification for different

samples was obtained by calculating the SPL and the particle velocity across the acoustic cavity when normal incident sound waves impinged on the cavity. The acoustic metamaterial was periodic; thus, we used a single unit cell with periodic boundary conditions for all of the calculations.

Measurement of the SPL gain inside the cavity in an underwater environment. In the underwater experiment, a spherical omnidirectional transducer (ITC-1001) and an underwater hydrophone (B&K 8103) were placed inside a $2 \times 1.5 \times 0.8$ m water tank. The source and the receiver were placed 0.2 and 0.1 m below the surface, respectively. A LFM chirp signal with a duration of 0.5 ms and a frequency range from 3 to 25 kHz with a 100-kHz sampling frequency was used as the source signal.

1. Kinsler, L. E., Frey, A. R., Coppens, A. B. & Sanders, J. V. *Fundamentals of Acoustics,* (Wiley, New York, 1999).
2. Sanches, J. M., Laine, A. F. & Suri, J. S. *Ultrasound Imaging,* (Springer, New York, 2011).
3. Kuperman, W. A. [Underwater Acoustics] *Springer Handbook of Acoustics* [Rossing, T.D. (ed.)] (Springer, New York, 2007).
4. Stojanovic, M. [Acoustic (Underwater) Communications] *Wiley Encyclopedia of Telecommunication* [Proakis, J.G. (ed.)] (Wiley, New York, 2002).
5. Kock, W. E. & Harvey, F. K. Refracting Sound Waves. *J. Acoust. Soc. Am.* **21**, 471 (1949).
6. Christensen, J. & Garcia de Abajo, F. J. Acoustic field enhancement and subwavelength imaging by coupling to slab waveguide modes. *Appl. Phys. Lett.* **97**, 164103 (2010).
7. Lemoult, F., Fink, M. & Lerosey, G. Acoustic resonators for far-field control of sound on a subwavelength scale. *Phys. Rev. Lett.* **107**, 064301 (2011).
8. Lemoult, F., Kaina, N., Fink, M. & Lerosey, G. Wave propagation control at the deep subwavelength scale in metamaterials. *Nat. Phys.* **9**, 55 (2013).
9. Zhu, J. *et al.* Acoustic rainbow trapping. *Sci. Rep.* **3**, 1728 (2013).
10. Colombi, A., Roux, P. & Rupin, M. Sub-wavelength energy trapping of elastic waves in a metamaterial. *J. Acoust. Soc. Am.* **136**, EL192 (2014).
11. Christensen, J., Garcia-Vidal, F. J., Martin-Moreno, L. & Zhu, J. A holey-structured metamaterial for acoustic deep-subwavelength imaging. *Nat. Phys.* **55**, 52–55 (2011).
12. Christensen, J. *et al.* Collimation of sound assisted by acoustic surface waves. *Nat. Phys.* **3**, 851–852 (2007).
13. Zigoneanu, L., Popa, B.-I. & Cummer, S. A. Three-dimensional broadband omnidirectional acoustic ground cloak. *Nat. Mater.* **13**, 352–355 (2014).
14. Christensen, J., Martin-Moreno, L. & Garcia-Vidal, F. J. All-angle blockage of sound by an acoustic double-fishnet metamaterial. *Appl. Phys. Lett.* **97**, 134106 (2010).
15. Liang, Z. & Li, J. Extreme acoustic metamaterial by coiling up space. *Phys. Rev. Lett.* **108**, 114301 (2012).
16. Liu, Z. Locally resonant sonic materials. *Science* **289**, 1734–1736 (2000).
17. Zhang, S., Xia, C. & Fang, N. Broadband acoustic cloak for ultrasound waves. *Phys. Rev. Lett.* **106**, 024301 (2011).
18. Fang, N. Ultrasonic metamaterials with negative modulus. *Nat. Mater.* **5**, 452–456 (2006).
19. Liang, Z., Willatzen, M., Li, J. & Christensen, J. Tunable acoustic double negativity metamaterial. *Sci. Rep.* **2**, 859 (2012).
20. D'Aguanno, G. *et al.* Broadband metamaterial for nonresonant matching of acoustic waves. *Sci. Rep.* **2**, 340 (2012).
21. Li, J. & Chan, C. T. Double-negative acoustic metamaterial. *Phys. Rev. E* **70**, 055602 (2004).
22. Lee, S. H., Park, C. M., Seo, Y. M., Wang, Z. G. & Kim, C. K. Composite Acoustic Medium with Simultaneously Negative Density and Modulus. *Phys. Rev. Lett.* **104**, 054301 (2010).
23. Zhu, J. *et al.* Acoustic rainbow trapping. *Sci. Rep.* **3**, 1728 (2013).
24. Ding, Y., Liu, Z., Qiu, C. & Shi, J. Metamaterial with Simultaneously Negative Bulk Modulus and Mass Density. *Phys. Rev. Lett.* **99**, 093904 (2007).
25. Fleury, R. & Alù, A. Extraordinary Sound Transmission through Density-Near-Zero Ultranarrow Channels. *Phys. Rev. Lett.* **111**, 055501 (2013).
26. Popa, B.-I. & Cummer, S. A. Non-reciprocal and highly nonlinear active acoustic metamaterials. *Nat. Commun.* **5**, 4398 (2014).
27. Pierre, J., Dollet, B. & Leroy, V. Resonant Acoustic Propagation and Negative Density in Liquid Foams. *Phys. Rev. Lett.* **112**, 148307 (2014).
28. Li, Y. *et al.* Unidirectional acoustic transmission through a prism with near-zero refractive index. *Appl. Phys. Lett.* **103**, 053505 (2013).
29. Li, J., Fok, L., Yin, X., Bartal, G. & Zhang, X. Experimental demonstration of an acoustic magnifying hyperlens. *Nat. Mater.* **8**, 931–934 (2009).
30. Song, K., Lee, S.-H., Kim, K., Hur, S. & Kim, J. Emission Enhancement of Sound Emitters using an Acoustic Metamaterial Cavity. *Sci. Rep.* **4**, 4165 (2014).
31. Liang, Z. *et al.* Space-coiling metamaterials with double negativity and conical dispersion. *Sci. Rep.* **3**, 1614 (2014).
32. Smith, D. R., Schultz, S., Markos, P. & Soukoulis, C. M. Determination of effective permittivity and permeability of metamaterials from reflection and transmission coefficients. *Phys. Rev. B* **65**, 195104 (2002).

33. Fokin, V., Ambati, M., Sun, C. & Zhang, X. Method for retrieving effective properties of locally resonant acoustic metamaterials. *Phys. Rev. B* **76**, 144302 (2007).

Acknowledgments

Author contributions

K.S. and J. K. designed the acoustic metamaterial for the SPL boost in the ultra-small cavity, and K.K., K.S., and J.K. carried out the SPL measurements in air. J.K., J.P., and J.R.Y. designed and tested the measurements of the SPL in the underwater environment. K.S., J. H. K., and S.H. performed the measurements of the SPL in the corridor. J.K. and K.S. conducted the numerical simulations and wrote the manuscript.

Additional information